Results in Surfaces and Interfaces 18 (2025) 100367

Contents lists available at ScienceDirect

Results in Surfaces and Interfaces

journal homepage: www.elsevier.com/locate/rsurfi

Mechanical and tribological characterization of polyamide 66/graphite nanocomposites

Tamiris de Paula Anjolleto [a], Daniel Eurico Salvador de Sousa [b], Francisco Vieira dos Santos [a], Marcia Cristina Branciforti [a,*]

[a] Department of Materials Engineering, Sao Carlos School of Engineering, University of Sao Paulo, Sao Carlos, SP, Brazil
[b] Department of Materials Engineering, Federal University of Sao Carlos, Sao Carlos, SP, Brazil

ARTICLE INFO

Keywords:
Polyamide 6.6
Nanographite
Hardness
Impact resistance
Wear resistance
Calotest method
Mechanical properties
Morphology
Tribology

ABSTRACT

Polymer nanocomposites can be employed in diverse engineering applications where wear is a critical concern. Understanding the mechanical and wear properties as applied to polymer nanocomposites is crucial for comprehending the behaviour of workpieces. In this study, three types of nanographites were incorporated at a concentration of 2.5 wt% into a polyamide 6.6 matrix. The graphites differ owing its production process. Tests of wear, impact, and elastic deformation resistance, hardness, and morphology were conducted to evaluate the performance of the PA66/graphite nanocomposites. All nanocomposites exhibit a homogeneous morphology with good dispersion, distribution, and orientation of the nanographites in the matrix, suggesting the effectiveness of the processing methods employed. The incorporation of 2.5 wt% of nanographites A, B, and C improved the wear resistance of PA66 by 52%, 74%, and 44%, respectively. The PA66/graphite nanocomposites exhibited an increase in Shore D hardness up to 2.8%, and in elastic modulus between 8.3% and 13.0%. The impact resistance of the nanocomposites decreased by 15.4%–21.3%. The results revealed that the production process of the nanographites impacted the performance of the produced nanocomposites.

1. Introduction

Polymeric materials, due to their low density and cost-effective processing, have replaced metallic and ceramic materials in various sectors, including aerospace, automotive, biomedical, microelectronic packaging, and coatings. Polymers are utilized either in their pure form or with additives added during processing to enhance physical, chemical, mechanical, and tribological properties, thereby rendering the material suitable for specific applications (Francis et al., 2014). In the field of tribology, polymers are increasingly utilized due to the elasticity of polymer chains, their wear resistance, and their low coefficients of friction (Sinha and Briscoe, 2009). Polymers such as polyamides, polytetrafluoroethylene, polyacetals, ultra-high molecular weight polyethylene, polyetheretherketone, polyurethanes, phenolic resins, and epoxy are attractive for engineering applications in which wear is a critical issue (Stachowiak and Batchelor, 2014). As an example, polyamide is an engineering polymer extensively employed in applications such as bearings, gears, cable sheathing, hoses, fibers, and conveyor belt reinforcement, owing to its excellent mechanical strength and wear resistance in comparison to other polymers. However, its susceptibility to moisture absorption and relatively low toughness restricts the range of applications for polyamide (Deopura et al., 2008; Meyer et al., 2002). Regarding water absorption by certain polymers, Yamamoto and Takashima (2002) assert that water molecules readily diffuse into the free volume of the amorphous phase of the polymer. This process leads to plasticization, swelling, and softening, resulting in decreased polymer hardness and strength. Additionally, water diffusion diminishes the forces of attraction between polymer chains, facilitating material removal during sliding, consequently accelerating the rate of wear. To mitigate these factors and enhance the tribological behavior of these polymers, various reinforcing fillers are commonly employed. Examples include zirconia, silicon carbide, titanium dioxide, and copper oxide (Bahadur and Sunkara, 2005), molybdenum disulfide (Ben Difallah et al., 2014), graphene (Masood et al., 2017), graphite (Shalwan and Yousif, 2014), and polytetrafluoroethylene (Burris and Sawyer, 2006). As an example, we emphasize graphite, a material extensively utilized as reinforcement in polymer matrices. Its inclusion in the polymeric matrix markedly enhances mechanical, thermal, and electrical properties.

* Corresponding author.
E-mail address: marciacb@sc.usp.br (M.C. Branciforti).

https://doi.org/10.1016/j.rsurfi.2024.100367
Received 17 August 2024; Received in revised form 19 November 2024; Accepted 23 November 2024
Available online 26 November 2024

Graphite can enhance dimensional stability and reduce water absorption in polyamides. Moreover, it boasts a high aspect ratio (100–500), facilitating dispersion within the polymeric matrix. With a modulus of elasticity of 1.000 MPa, graphite exhibits properties akin to carbon, graphene, and fullerene nanotubes but at a significantly lower cost (Goyal et al., 2008; Goyal and Yadav, 2014; Li et al., 2018). In this context, Gong et al. (2017) fabricated a nanostructured graphite/molybdenum disulfide film with super lubricity. This film was applied to reduce wear and friction, which are major contributors to damage in mechanical components during service.

According to Jawaid et al. (2018), the introduction of fillers into the polymeric matrix enhances mechanical and thermal properties, as well as wear rate and friction coefficient. Specifically, mechanical properties such hardness, tensile strength, stiffness, and impact resistance are affected positively. Moreover, thermal properties such as thermal conductivity and coefficient of expansion are influenced. Unal and Mimaroglu (2012) showed that the wear rate of polyamide 6 and polyamide 6/graphite (5 and 15 wt%) is highly influenced by sliding speed, and the coefficient of friction increases with the increasing load and sliding speed values.

Therefore, composite materials represent a viable alternative, as they possess the capability to tailor their properties by adjusting the reinforcement ratio within the matrix. Moreover, these materials have found widespread use across industries such as aerospace, automotive, and chemicals, displacing traditional ceramics and metal alloys, particularly in applications necessitating reduced noise, enhanced corrosion resistance, abrasion resistance, self-lubrication, and a high strength-to-weight ratio (Jawaid et al., 2018; Mcelwain et al., 2008). Thus, the performance of these novel materials is heavily reliant on the interface between the matrix and reinforcements. Inadequate surface interactions can lead to insufficient stress transfer to the reinforcement or promote crack propagation. Consequently, many of these reinforcements undergo surface treatments before composite fabrication. Furthermore, such treatments can enhance chemical resistance, particularly for metal particles prone to rapid oxidation. Processing methods also significantly influence the development of an effective material by affecting the dispersion and distribution of the reinforcement, thereby contributing to a homogeneous material, especially in the case of highly agglomerated nanoparticles (Jawaid et al., 2018; Faes et al., 2015).

Friedrich (2018) emphasizes that numerous polymer composites have been employed in diverse engineering applications where wear and friction are significant concerns. The author further asserts that comprehending tribology as applied to polymer composites is crucial for understanding the behavior of workpieces. This understanding is particularly vital as the addition of reinforcement to the polymeric matrix, whether in the form of nanoparticles or traditional fillers, will influence the wear performance of the composite. Zhou et al. (2019) employed graphite and graphene (3D) platelets as reinforcements in an epoxy resin matrix to enhance thermal conduction and wear resistance of the polymeric matrix. The synergy between graphite and graphene resulted in a 258% increase in thermal conduction, and the wear resistance surpassed that achieved when using graphite or graphene alone in the polymer matrix. Lingesh et al. (2018) investigated the incorporation of molybdenum disulfide (MoS_2), silicon carbide (SiC), and alumina (Al_2O_3) on a micrometer scale into the polyamide 6.6/polypropylene (PA66/PP) matrix. To this end, three types of composites were produced: PA66/PP/MoS_2, PA66/PP/MoS_2/SiC, and PA66/PP/MoS_2/SiC/Al_2O_3. The tribological analysis revealed that the abrasion wear of the produced composites is contingent upon the type of filler (both size and composition) as well as the abrasion distance. In terms of wear, the PA66/PP/MoS_2 composite exhibited the lowest wear volume loss and the lowest specific wear rate. Sekhar and Varghese (2019) examined the effects of incorporating intercalated graphite and natural graphite into a phenolic resin polymer matrix on mechanical, thermal, and rheological properties. Three composites with varying concentrations of intercalated graphite were prepared. The findings indicated that the addition of intercalated graphite enhanced the mechanical and thermal properties of the phenolic resin compared to the incorporation of natural graphite. The rheological study revealed that regardless of the graphite type, viscosity increased with higher graphite content in the polymeric matrix. At elevated graphite concentrations, the rheological behavior observed in the composites was pseudoplastic and thixotropic. Gheisari and Polycarpou (2019) analyzed the tribological behavior of polyimide (PI) and polytetrafluoroethylene (PTFE) polymers following the incorporation of powdered or flake graphite. The physical shape of the graphite notably impacted the performance of the produced composites in terms of wear and friction. For flake graphite, the highest wear and friction values were observed for the PTFE composite compared to the PI composite. This was attributed to the larger particle size of the flake form compared to the powdered form. However, both composites exhibited acceptable wear rates when compared to polyetheretherketone (PEEK). Rudresh and Ravikumar (2018) examined the abrasive wear behavior of the PA66/PTFE blend using the rubber wheel abrasion test. The results indicated that abrasive wear is affected by factors such as load shape, blend composition, and abrasion distance. The incorporation of 5 wt% PTFE improved the wear resistance of the blend, while the addition of 30 wt% PTFE led to a 40% reduction in material loss due to wear. The current study aimed to address the industrial demand for acquiring knowledge about the fabrication technology of new composite materials. Additionally, it sought to evaluate the performance of the samples in wear test and propose a potential replacement for metallic materials in tribological applications. For this purpose, this study investigated the wear resistance of PA66 incorporated with three types of nanographite obtained by different methods. The characterization tests aimed to understand how the incorporation of three types of nanographites affects the performance of PA66. To achieve this, tests of wear, hardness, impact resistance, tensile and morphology analysis were conducted.

2. Materials and methods

2.1. Materials

The polymeric matrix used was polyamide 6.6 (PA66) Technyl A216, produced by Rhodia Polyamides & Specialties. It had a molar mass of 8,500 g/mol, a melting temperature (Tm) of 263 °C, and a density of 1.144 g/cm^3. Two types of nanographites, labeled A and B, were obtained through high-energy milling of conventional graphite manufactured by Nacional de Graphite. Nanographite type B had a very low fraction (<1%) of micrographite remaining during the milling process and contains silicon carbide. Nanographite C was an expanded nanographite, Micrograf HC11, also manufactured by Nacional de Graphite with a plateled diameter of around 50 nm, and with the highest surface area among the nanographites. Its manufacturing process involved intercalation followed by thermal expansion. The physical properties of the nanographites were withheld due to industrial confidentiality.

2.2. Processing of the PA66/graphite nanocomposites

The PA66/graphite nanocomposites underwent a five-stage processing method (Lucas et al.): 1) Pre-melting of the PA66. 2) Combination of the polymer with expanded graphite in proportion of 10 wt% in a thermo-kinetic mixer to create nanocomposites with a high aspect ratio. 3) Recovery of the melted material. 4) The PA66/graphite nanocomposites with 2.5 wt% of each nanographite were processed using a co-rotating interpenetrating twin-screw extruder manufactured by Imacom. The extruder had a 35 mm screw diameter and a length-to-diameter ratio (L/D) of 44. Two types of side feeders, gravimetric and volumetric, were utilized. The screw profile was specifically designed for manufacturing nanocomposites and included conveying elements, reverse elements, idle-mixture, and turbine elements. Table 1 illustrates the composition of each studied nanocomposites.

Table 1
Composition of the PA66/graphite nanocomposites.

Sample	Polyamide 6.6 (wt.%)	Nanographite (wt.%)
PA66	100	0
PA66 + 2.5%A	97.5	A – 2.5
PA66 + 2.5%B	97.5	B – 2.5
PA66 + 2.5%C	97.5	C – 2.5

5) The injection molding process was employed to produce the samples for the tests. The mold features two cavities: one for tensile testing and the other for impact testing, with dimensions specified according to ASTM D638-14 (ASTM D638 – 14, 2014) and ASTM D256-10 (ASTM D256 – 10, 2010) standards, respectively. The machine utilized was an Arburg All-rounder 270 V, with a closing force of 300 kN and a screw diameter of 120 mm. The cooling system was controlled by an HB W 140 unit, manufactured by HB Therm.

2.3. Density determination

The density of the materials was determined using a pycnometer, with distilled water as the reference fluid, which has a density of 0.9995 g/cm^3 at 24 °C. Ten specimens of each sample were tested to calculate the average density.

2.4. Wear testing

The wear performance of the produced nanocomposites was evaluated using the calotest method. John F. Archard proposed a simple model to predict volume loss due to wear, represented as wear rate (Q) in mm^3/m, as shown in Equation (1). Hardness (H) is regarded as the most significant factor in wear control, with higher hardness resulting in lower wear rates. The applied normal pressure (W) is expressed in kg. m^{-1}. s^{-2}, and K (dimensionless) represents the Archard wear number. However, this model is effective primarily for homogeneous materials experiencing adhesive wear. In the case of coated materials, the wear rate (Q) changes once the substrate is reached (Archard, 1953).

$$Q = K\frac{W}{H} \tag{1}$$

The main challenge of this model is to understand the load distribution across the surface, which generally cannot be predicted. Therefore, some wear tests employ an ideally non-deformable and very hard metallic sphere that generates wear marks. These marks have their volume or area easily calculated, providing insight into the applied load.

The wear testing apparatus comprises a metallic sphere with a 1-inch diameter rotating against a smooth flat surface, resulting in material removal in a cap-shaped form. This setup allows for the scratch volume to be easily and directly calculated by measuring the diameter of the wear mark. In contrast, other methods such as “pin on disc” and “rubber wheel sand” require converting the removed mass to volume. The contact between the metallic sphere and the material is enforced by weights attached to the apparatus, enabling the adjustment of various parameters to analyze the behavior of a material. The following equations (Equations (2)–(4)) outline how to calculate the wear rate, Q, based on the sphere radius (R), the duration of the test (t), the frequency of rotation of the machine (f), and the diameter of the crater (D).

Initially, the distance travelled of the sphere on the surface (S) can be calculated by Equation (2):

$$S = 2\pi Rtf \tag{2}$$

Then, the removed volume, V, can be calculated by Equation (3) knowing D and R.

$$V = \frac{\pi D^4}{64R} \tag{3}$$

And finally, the wear rate (Q) can be calculated by Equation (4), knowing V and S.

$$Q = \frac{V}{S} \tag{4}$$

In sliding wear tests, the counter bodies must be analyzed in terms of microstructure, wear rate, wear appearances, and wear mechanisms; the performance of the entire tribosystem plays a crucial role in sliding wear. The wear tests were conducted at temperatures around 23 °C without humidity control, and no lubricants or abrasive solutions were employed. Surface treatment was also not applied to preserve the frozen layer from the injection molding process, thus evaluating the surface as provided from manufacturing. The parameters were selected based on previous tests and references. The duration of the test was set to 5, 10, and 20 min, with a weight of 600 g and a speed of 300 RPM, ensuring a stable contact between the metal sphere and the material specimens. Authors noted a greater influence of sliding speed rather than load on the wear rate of a material. Additionally, for higher loads, the roughness of polymers will have less influence on wear rate (Unal and Mimaroglu, 2012). Prior to each test, the metal sphere (made of SAE 52100) was cleaned with a disposable cloth and ethanol. A virgin sphere was used for each test. After the test, both bodies (metal spheres and specimens) were analyzed, and their wear marks were measured using optical microscopy (OM) Olympus model BX60M microscope. Ten specimens of each composition were tested under the same wear test conditions. Therefore, the wear results consider the combined wear rates of the entire tribological system, including both metal spheres and specimens, based on ten measurements of each sample under a given condition.

2.5. Hardness testing

The hardness tests were carried out in accordance with the ASTM D2240 - 05(2010) Standard Test Method for Rubber Property - Durometer Hardness (ASTM D2240 – 05, 2005). The recommended scale for these materials is the Shore D scale, with reliable values ranging from 20 to 90. An analog Zwick durometer was employed to conduct 10 measurements for each sample, with an exposure time of 15 s.

2.6. Tensile testing

The tensile tests were conducted in accordance with the ASTM D638 – 10 Standard Test Method for Tensile Properties of Plastics (ASTM D638 – 14, 2014). To obtain the elastic modulus, an extensometer was utilized at the rupture region to measure displacement. The results obtained correspond to the tension and displacement at 0.05 % and 0.5 % of displacement, with a testing speed set to 5 mm/min. The equipment used was an INSTRON model 5569, and 10 specimens of each sample were tested to calculate the average modulus.

2.7. Impact testing

The tests were carried out following the procedures outlined in the ASTM D256 – 10 Standard Test Methods for Determining the Izod Pendulum Impact Resistance of Plastics (ASTM D256 – 10, 2010), including sample conditioning and the application of Method A for notched specimens. The CEAST model RESIL 25 R equipment, with a hammer releasing 2 J of energy, was used. The energy loss due to friction was measured at 0.024 J. To determine the average impact strength for each material, 10 specimens of each sample were tested.

2.8. Scanning electron microscopy (SEM)

SEM analysis was conducted to observe the dispersion and distribution of nanographite throughout the polymer matrix and to evaluate its interface. Liquid nitrogen was employed to fracture the samples, ensuring a suitable surface for observation. Subsequently, the samples

were affixed to a support using conductive glue and coated with a thin layer of gold. Three specimens of each sample were analyzed. A Phillips microscope XL30 was utilized, operating at 10 kV energy.

3. Results and discussions

3.1. Density determination

The density measurements indicated average density values of 1.162 g/cm^3, 1.162 g/cm^3, and 1.164 g/cm^3 (±0.001 at 24°C) for the PA66 + 2.5%A, PA66 + 2.5%B, and PA66 + 2.5%C nanocomposites, respectively, that represents an average increase of 1.63% compared to PA66 sample (1,144 g/cm^3).

3.2. Wear testing

The diameter of wear images was measured using Image-Pro®Plus software. Fig. 1 display optical microscopy (OM) images of wear testing conducted on PA66, PA66 + 2.5%A, PA66 + 2.5%B, and PA66 + 2.5%C samples, utilizing a weight of 600 g and lasting for a duration of 20 min.

As can be observed in the optical microscopy images, Fig. 1, wear creates deeper marks, as shown in Fig. 1(a) and (b), the worn surfaces appear heterogeneous. Achieving a perfect circle is challenging due to several factors, including: Gathering of residues on the borders of the removed mark during the cleaning process, resulting in the formation of craters as depicted in Fig. 1(d) by the red arrow; Loss of mechanical resistance due to heat generated from the friction between the sphere and the material, causing localized regions to easily reach their glass transition temperature (Tg) (for PA66, Tg is approximately 50 °C (Sinha and Briscoe, 2009; Unal and Mimaroglu, 2012)); Presence of third-party materials, combining adhesive and abrasive wear, originating from the environment or as debris from the material; No surface polishing was employed, leading to variations in wear across the surface.

For thermoplastics, when in attrition with metals, there is a tendency to create polymer transfer films to the other material, reducing the friction coefficient and consequently wear rate of the material. Hence, for this test this adherence to the sphere creates a polymer "ring". The opposite happens for harder materials, since the sphere will also suffer wear, providing shallower marks due its circular wear. Fig. 2 schematically represents this phenomenon.

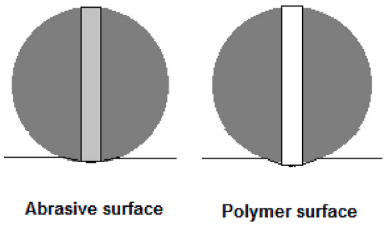

Fig. 2. Schematic representation of adhesive wear on abrasive and polymer surfaces.

In the materials studied, no transfer/adherence of material between the body and the counterbody, or vise-versa was observed by optical microscopy analysis. The metal sphere's surfaces showed no microstructural changes or surface alteration, such as wear, marks, or even changes in weight. Thus, the wear on the counterbody was considered negligible throughout the entire tribosystem.

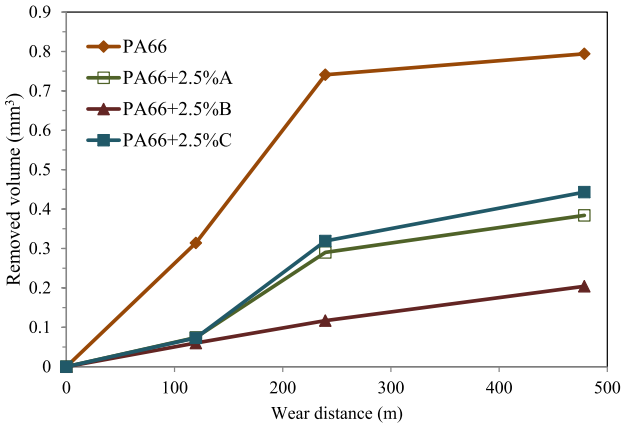

Fig. 3. Wear removed volume versus wear distance using 600 g weight.

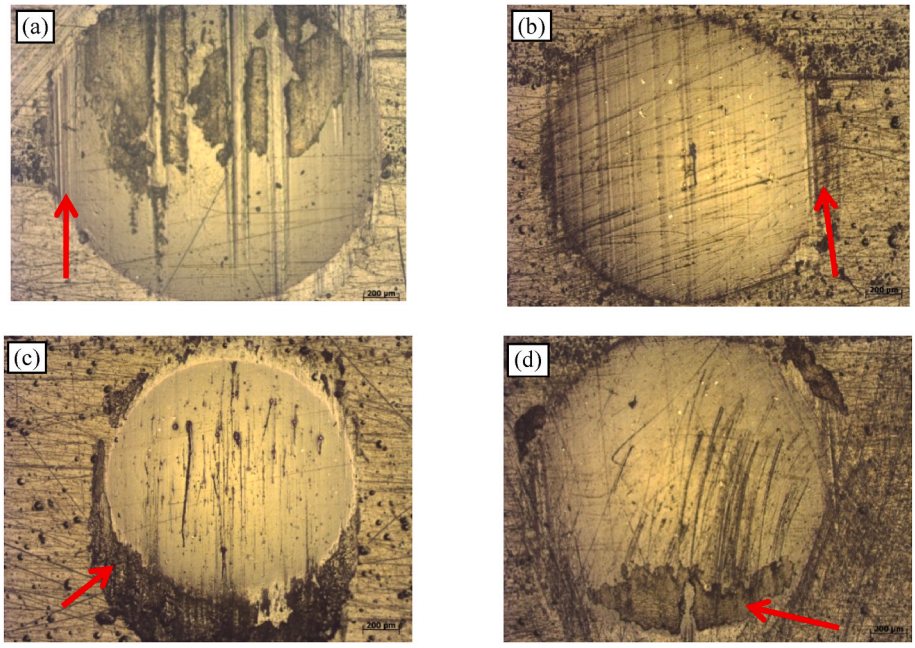

Fig. 1. Optical microscopy images of wear testing conducted on (a) PA66, (b) PA66 + 2.5%A, (c) PA66 + 2.5%B, and (d) PA66 + 2.5%C samples, using 600 g weight for 20 min.

Fig. 3 presents the results of the wear test conducted on PA66 and PA66/graphite nanocomposites, utilizing a weight of 600 g. The average percentage of removed volume of wear in mm^3 ratios of the nanocomposites based on the PA66 sample was calculated and the standard deviation of the measurements was between $\pm 7.33 \times 10^{-4}$ and 4.03×10^{-5}. Negative percentages of removed volume indicate a reduction in wear, thus indicating an improvement in the wear resistance of the material.

PA66 + 2.5%B nanocomposite displays a −74% reduction in the worn volume, which exhibited the best performance among the others. PA66 + 2.5%A and PA66 + 2.5%B nanocomposites showed a −52% and −44% reduction in wear. Despite undergoing the same procedures, samples with nanographites type A and B showed differing wear resistance due to the addition of silicon carbide to type B. For high wear distance, the PA66 + 2.5%A nanocomposite shows a −12% reduction in the worn volume in comparison to PA66 + 2.5%C nanocomposite. Additionally, there is an observed tendency for the wear volume rate (Q) to decrease. This tendency cannot be solely attributed to lubrication from the addition of graphite, as the same trend is observed for the virgin material. A possible explanation could be the formation of a polymer transfer film during the test.

For PA66/graphite nanocomposites, it was anticipated that the layers of graphite, held together by weak van der Waals bonds, would be susceptible to shearing under load induced by sliding. The abundance of flakes present in the debris would form a film on the counterpart, such as on the metal ball, thereby reducing adhesion and consequently resulting in a decrease in the wear rate and friction coefficient (Chang et al., 2006). The wear mechanism of polyamide 6/graphite composites includes transferred film and deformation and adhesive wear processes (Unal and Mimaroglu, 2012).

3.3. Hardness testing

Fig. 4 shows the average value and standard deviation of Shore D hardness results of PA66 and PA66/graphite nanocomposite samples.

The increase in hardness due to the addition of nanographites was approximately 3%. The hardest sample was found to be the nanocomposite containing nanographite C. This behavior is probably due to the higher surface area of nanographite C compared to nanographites A and B. The larger surface area of the nanographite particles may provide better charge distribution and increased interaction between the particles and the polymer matrix, hindering the movement of dislocations and deformations, which could result in an increase in the composite's hardness. Unal and Mimaroglu (2012) reported values of 75 and 78 Shore D for PA6 and PA6 with 5 wt% graphite, respectively, which are higher than those obtained for PA66 + 2.5%C nanocomposites.

3.4. Tensile testing

The obtained elastic modulus (E) for the tensile testing is depicted in Fig. 5. Similar to the other tests presented, the average elastic modulus value obtained for the pure material (PA66 sample) was utilized as a reference, enabling easy observation of improvement or deterioration.

An increase in the elastic modulus is observed for all the nanocomposites, with PA66 + 2.5%C exhibiting the highest performance among these materials. Comparing samples PA66 + 2.5%A and PA66 + 2.5%B, it can be assumed that the addition of silicon carbide to the process decreases the Young's modulus. Unal and Mimaroglu (2012) reported elastic moduli of 2.8 and 3.4 GPa for PA6 and PA6 with 5 wt% graphite, respectively, all of which are lower than those observed for the nanographites studied in this research.

According to Li and Zhong (2011), the incorporation of graphite nanoplatelets can alter the behavior of the modulus of elasticity in three ways: (1) stress reduction with an increase in incorporated load; (2) increased stress with an increase in incorporated load; and (3) stress reaching a maximum value and then decreasing with increasing load incorporation. Additionally, Meng (2006) states that tensile strength and Young's modulus have been demonstrated to be significantly improved in polymer/graphite nanocomposites.

3.5. Impact testing

The results obtained for the Izod impact testing of PA66 and PA66/graphite nanocomposite samples are presented in Fig. 6.

A decrease was anticipated for all nanocomposite samples compared to the PA66 sample due to their higher elastic modulus, which renders the material more brittle and less shock-absorbent. Swallowe (1999) reports an impact resistance of 50 J/m^2 for PA66. Unal and Mimaroglu (2012) reported impact strengths of 7.8 and 9.2 kJ/m^2 for polyamide 6 and polyamide 6 with 5 wt% graphite, respectively, significantly higher than the materials studied in this research due to the better impact resistance of polyamide 6 in comparison to polyamide 6.6.

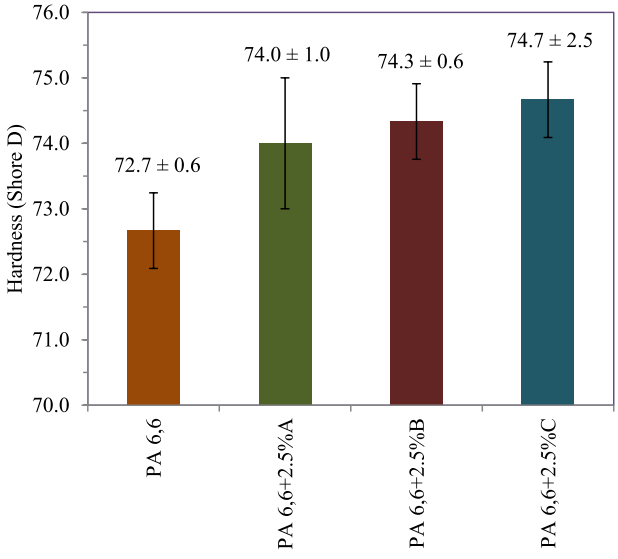

Fig. 4. Shore D hardness of PA66 and PA66/graphite nanocomposites.

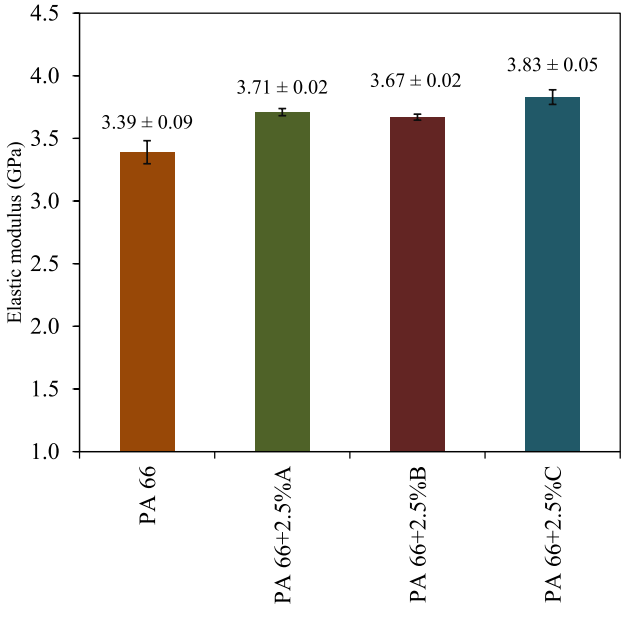

Fig. 5. Elastic modulus of PA66 and PA66/graphite nanocomposites.

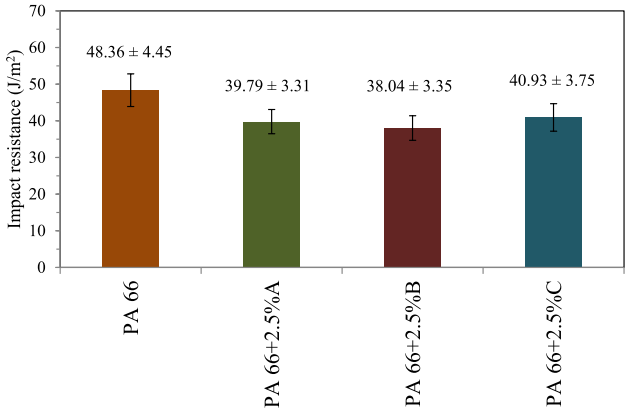

Fig. 6. Izod impact resistance of PA66 and PA66/graphite nanocomposites.

Surprisingly, among the PA66/graphite nanocomposites, sample PA66 + 2.5%C exhibited the highest results for both impact strength and elastic modulus. It is known that graphite C has approximately three times more surface area than the other graphite types used in this study, which would lead to a higher nucleation of spherulites during the material cooling process. With higher crystallinity, the material typically demonstrates better results for both elastic modulus and impact strength.

3.6. Scanning electron microscopy (SEM)

SEM images were captured to assess the interface between the matrix and the fillers, as well as to evaluate the distribution and dispersion of the fillers within the matrix. Figs. 7 and 8 show SEM images of PA66 and PA66/graphite nanocomposites with higher and lower magnifications, respectively.

The MEV micrographs presented in Fig. 7 demonstrate the excellent interface between the PA66 matrix and all nanographites, indicated by red arrows, corroborating the previously discussed results. Additionally, the SEM images reveal that, although the nanographites have similar plate morphologies, type C nanographite has a larger surface area (as indicated by blue arrow) compared to the other nanographites. Preliminary results of Brunauer-Emmett-Teller (BET) measurements revealed that type C graphite has a surface area three times greater than that A and B types graphites, due to its production process.

As shown in Fig. 8, SEM micrographs at lower magnification reveal a preferential orientation of the nanographites (indicated by the orange arrows), which is likely expected due to the processing method (injection molding) used to obtain the nanocomposites. This orientation contributes to the anisotropy of the material.

Finally, Fig. 9 shows the hardness, impact, tensile, and wear resistance result ratios of PA66/graphite nanocomposites based on PA66 reference sample. The zero-line representing the reference sample. Negative values in the wear test indicate an increase in wear resistance.

For all nanocomposite samples an increase of elastic modulus, Shore D hardness and wear resistance was found, followed by the decay of impact strength. Which is consistent, since greater hardness and strength implies a drop of its tenacity, for this case it happened in a larger proportion for the latter.

As previously mentioned, sample PA66 + 2.5%C exhibits the highest elastic modulus, hardness, and impact strength among the nanocomposite samples. These results are attributed to the crystallinity of the material, which increases when more nucleation sites are provided, as depicted in Fig. 8, demonstrating better distribution and dispersion of the nanographite type C.

Comparing the PA66 + 2.5%A and PA66 + 2.5%B nanocomposites, the former exhibits higher elastic modulus. The only difference between them is the presence of silicon carbide in the processing of the B nanographite. Therefore, the presence of silicon carbide decreased the stiffness of the nanocomposite; this decrease is due to factors such as poor silicon carbide-polymer matrix interaction, particle dispersion, particle size, and the resulting composite structure.

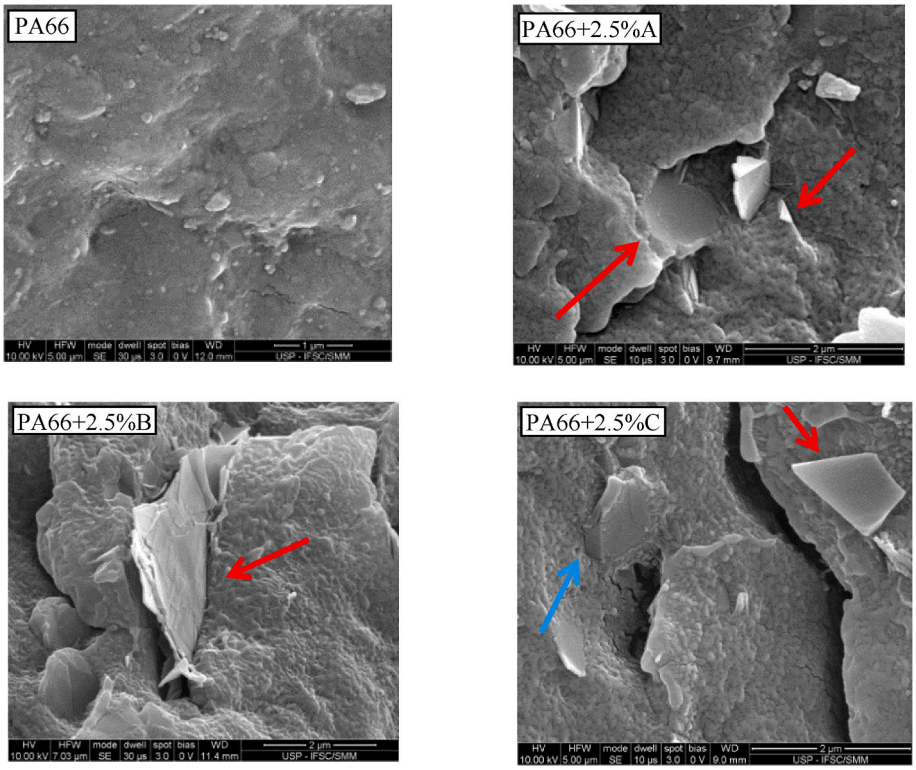

Fig. 7. SEM images at higher magnification of PA66, PA66 + 2.5 wt%A, PA66 + 2.5 wt%B, and PA66 + 2.5 wt%C nanocomposites.

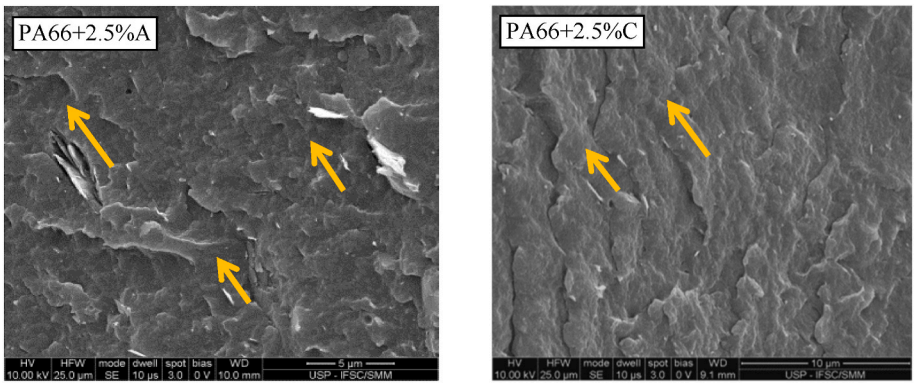

Fig. 8. SEM images at lower magnification of PA66 + 2.5 wt%A and PA66 + 2.5 wt%C nanocomposites.

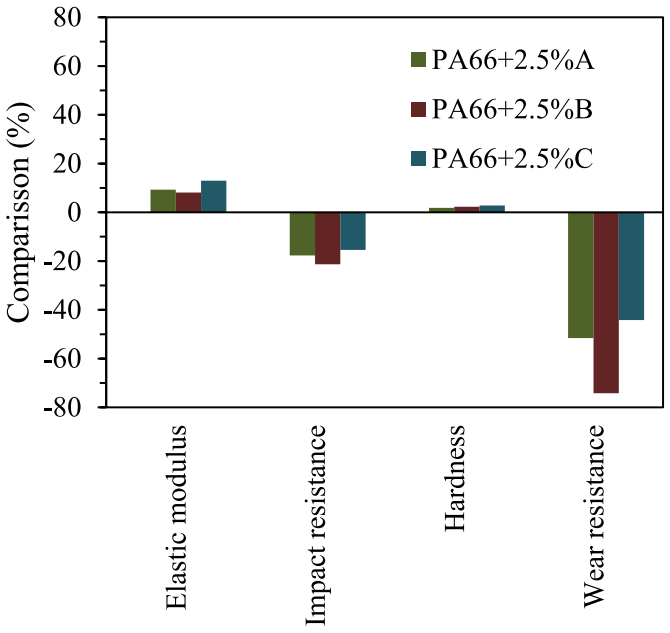

Fig. 9. Elastic modulus, impact resistance, Shore D hardness, and wear resistance ratios of PA66/graphite nanocomposites compared to PA66 sample.

Additionally, in the wear tests, the PA66 + 2.5%B nanocomposites exhibited the greatest improvement in wear resistance. It was initially anticipated that the sample with C nanographite would perform the best due to its greater hardness and elastic modulus. However, surprisingly, PA66 + 2.5%B, followed by PA66 + 2.5%A, showed better wear resistance results than the PA66 + 2.5%C nanocomposites. Therefore, it can be concluded that the production of A and B nanographite types, which are less expensive than type C, are better choices to achieve superior wear-resistant nanocomposites.

4. Conclusions

This study presents the wear and mechanical behaviors of PA66 incorporated with three types of nanographite obtained by different methods. The characterizations aimed to understand how the incorporation of the nanographites affects the wear resistance, hardness, impact resistance, morphology, and the rigidity performance of PA66/graphite nanocomposites. The nanographites B and C showed the best performance, with the former exhibiting higher wear resistance and the latter showing higher hardness, impact resistance, and strength. In general, the tests demonstrated the accuracy of properties affected by the addition of nanographite, such as increased rigidity and hardness, and a decrease in impact strength. As predicted by the Archard equation, these behaviors resulted in superior wear resistance. The wear modeling and prediction for nanocomposites is even more complex than for polymers, especially when considering the effects of lubricants and abrasives. However, this complexity does not diminish their desirability for wear applications, particularly in cases where easy processing, corrosion resistance, lightweight, and low-cost materials are priorities.

CRediT authorship contribution statement

Tamiris de Paula Anjolleto: Writing – original draft, Methodology, Investigation, Formal analysis. **Daniel Eurico Salvador de Sousa:** Writing – review & editing, Writing – original draft, Methodology, Investigation, Formal analysis, Data curation, Conceptualization. **Francisco Vieira dos Santos:** Writing – original draft, Visualization, Validation, Data curation. **Marcia Cristina Branciforti:** Writing – review & editing, Writing – original draft, Supervision, Resources, Project administration, Methodology, Funding acquisition, Conceptualization.

Declaration of competing interest

The authors declare that they have no known competing financial interests or personal relationships that could have appeared to influence the work reported in this paper.

Acknowledgements

The authors acknowledge the Coordination of Higher-Level Staff Improvement (CAPES, finance code 001) for the financial support and express their gratitude to Professor Luiz Carlos Casteletti for granting access to the wear apparatus. They also extend their appreciation to the MHNano company and its members for supplying the nanographites and engaging in valuable discussions and information sharing.

Data availability

Data will be made available on request.

References

Archard, J.F., 1953. Contact and rubbing of flat surfaces. J. Appl. Phys. 24 (8), 981–988. https://doi.org/10.1063/1.1721448.
ASTM D2240 – 05, 2005. American Society for Testing and Materials. Standard test method for rubber property-durometer hardness. Annu. Book ASTM Stand.
ASTM D256 – 10, 2010. American Society for Testing and Materials. Standard test method for determining the Izod Pendulum impact resistance of Plastics. Annu. Book ASTM Stand.
ASTM D638 – 14, 2014. American society for Testing and Materials. Standard test method for tensile properties of Plastics. Annu. Book ASTM Stand.
Bahadur, S., Sunkara, C., 2005. Effect of transfer film structure, composition and bonding on the tribological behavior of polyphenylene sulfide filled with nano particles of

TiO2, ZnO, CuO and SiC. Wear 258 (9), 1411–1421. https://doi.org/10.1016/j.wear.2004.08.009.
Ben Difallah, B., Kharrat, M., Dammak, M., Monteil, G., 2014. Improvement in the tribological performance of polycarbonate via the incorporation of molybdenum disulfide particles. Tribol. Trans. 57 (5), 806–813. https://doi.org/10.1080/10402004.2014.913751.
Burris, D.L., Sawyer, W.G., 2006. Improved wear resistance in alumina-PTFE nanocomposites with irregular shaped nanoparticles. Wear 260 (7–8), 915–918. https://doi.org/10.1016/J.WEAR.2005.06.009.
Chang, L., Zhang, H., Schlarb, A.K., 2006. On the sliding wear of nanoparticle filled polyamide 66 composites. Compos. Sci. Technol. 66 (16), 3188–3198. https://doi.org/10.1016/j.compscitech.2005.02.021.
Deopura, B.L., Alagirusamy, R., Joshi, M., Gupta, B., 2008. Polyesters and Polyamides, first ed. Woodhead Publishing Limited.
Faes, J.C., Rezaei, A., Van Paepegem, W., Degrieck, J., 2015. Influence of matrix toughness and interfacial strength on the toughness of epoxy composites with ductile steel fabric reinforcement. Compos. Interfac. 22 (8), 779–793. https://doi.org/10.1080/09276440.2015.1076639.
Francis, R., Joy, N., Aparna, E.P., Vijayan, R., 2014. School of chemic polymer grafted inorganic nanoparticles, preparation, properties, and applications: a review. Polym. Rev. 54 (2), 268–347. https://doi.org/10.1080/15583724.2013.870573.
Friedrich, K., 2018. Polymer composites for tribological applications. Adv. Ind. Eng. Polym. Res. 1 (1), 3–39. https://doi.org/10.1016/j.aiepr.2018.05.001.
Gheisari, R., Polycarpou, A.A., 2019. Tribological performance of graphite-filled polyimide and PTFE composites in oil-lubricated three-body abrasive conditions. Wear 436–437, 203044. https://doi.org/10.1016/j.wear.2019.203044.
Gong, Z., Jia, X., Ma, W., Zhang, B., Zhang, J., 2017. Hierarchical structure graphitic-like/MoS 2 film as superlubricity material. Appl. Surf. Sci. 413, 381–386. https://doi.org/10.1016/j.apsusc.2017.04.057.
Goyal, R.K., Yadav, M., 2014. The wear and friction behavior of novel polytetrafluoroethylene/expanded graphite nanocomposites for tribology application. J. Tribol. 136 (2), 1–5. https://doi.org/10.1115/1.4025655.
Goyal, R., Jagadale, P., Mulik, U., 2008. Thermal, mechanical, and dielectric properties of polystyrene/expanded graphite nanocomposites. J. Appl. Polym. Sci. 111 (5), 2071–2077. https://doi.org/10.1002/app.29042.
Jawaid, M., Nagarajan, R., Sukumaran, J., De Baets, P., 2018. Synthesis and Tribological Applications of Hybrid Materials, first ed. Wiley-VCH.
Li, B., Zhong, W.H., 2011. Review on polymer/graphite nanoplatelet nanocomposites. J. Mater. Sci. 46 (17), 5595–5614. https://doi.org/10.1007/s10853-011-5572-y.
Li, J., Ge, X., Luo, J., 2018. Random occurrence of macroscale superlubricity of graphite enabled by tribo-transfer of multilayer graphene nanoflakes. Carbon 138, 154–160. https://doi.org/10.1016/j.carbon.2018.06.001.
Lingesh, B.V., Ravi Kumar, B.N., Rudresh, B.M., Reddappa, H.N., 2018. Effect of micro fillers on two body abrasive wear behavior of polyamide 66 and polypropylene (PA66/PP) blend based composites. Mater. Today: Proc. 5 (10), 22376–22383. https://doi.org/10.1016/j.matpr.2018.06.605. Part 3.
Lucas, A. A.; Branciforti, M. C.; Sousa, D. E. S. Obtaining conductive polymeric nanocomposites: production process and nanocomposites obtained thus. Patent: Innovation Privilege. Registration Number PI1020120077469. National Institute of Industrial Property (INPI). Deposit at 04/09/2012, Brazil.
Masood, M.T., Papadopoulou, E.L., Heredia-Guerrero, J.A., Bayer, I.S., Athanassiou, A., Ceseracciu, L., 2017. Graphene and polytetrafluoroethylene synergistically improve the tribological properties and adhesion of nylon 66 coatings. Carbon 123, 26–33. https://doi.org/10.1016/j.carbon.2017.07.026.
Mcelwain, S.E., Blanchet, T.A., Schadler, L.S., Sawyer, W.G., 2008. Effect of particle size on the wear resistance of alumina-filled PTFE micro- and nanocomposites. Tribol. Trans. 51 (3), 247–253. https://doi.org/10.1080/10402000701730494.
Meng, Y., 2006. Polymer/graphite nanocomposites. In: Polymer Nanocomposites, second ed., 19. Woodhead Publishing Cambridge, pp. 510–539.
Meyer, A., Jones, N., Lin, Y., Kranbuehl, D., 2002. Characterizing and modeling the hydrolysis of polyamide-11 in a pH 7 water environment. Macromolecules 35 (7), 2784–2798. https://doi.org/10.1021/ma010541o.
Rudresh, B.M., Ravikumar, B.N., 2018. Investigation on three body abrasive wear behavior of polyamide66/polytetrafluroethylene (PA66/PTFE) blends. Mater. Today: Proc. 5 (1), 2503–2511. https://doi.org/10.1016/j.matpr.2017.11.032. Part 3.
Sekhar, N.C., Varghese, L.A., 2019. Mechanical, thermal, and rheological studies of phenolic resin modified with intercalated graphite prepared via liquid phase intercalation. Polym. Test. 79, 106010. https://doi.org/10.1016/j.polymertesting.2019.106010.
Shalwan, A., Yousif, B.F., 2014. Influence of date palm fibre and graphite filler on mechanical and wear characteristics of epoxy composites. Mater. Des. 59, 264–273. https://doi.org/10.1016/j.matdes.2014.02.066.
Sinha, S.K., Briscoe, B.J., 2009. Polymer Tribology, first ed. London Imperial College Press.
Stachowiak, G.W., Batchelor, A.W., 2014. Engineering Tribology, fourth ed. Butterworth-Heinemann.
Swallowe, G.M., 1999. Mechanical Properties and Testing of Polymers, vol. 3. Springer, p. 302.
Unal, H., Mimaroglu, A., 2012. Friction and wear performance of polyamide 6 and graphite and wax polyamide 6 composites under dry sliding conditions. Wear 289, 132–137. https://doi.org/10.1016/j.wear.2012.04.004.
Yamamoto, Y., Takashima, T., 2002. Friction and wear of water lubricated PEEK and PPS sliding contacts. Wear 253 (7–8), 820–826. https://doi.org/10.1016/S0043-1648(02)00059-5.
Zhou, H., Wang, H., Du, X., Mo, Y., Yuan, H., Liu, H.-Y., 2019. Hybrid three-dimensional graphene fillers and graphite platelets to improve the thermal conductivity and wear performance of epoxy composites. Compos. Appl. Sci. Manuf. 123, 270–277. https://doi.org/10.1016/j.compositesa.2019.05.016.